Research Article

Modeling the Liquid-Phase Adsorption of Cephalexin onto Coated Iron Nanoparticles Using Response Surface and Molecular Modeling

Shabnam Ahmadi [ID],[1] **Soumya Ghosh** [ID],[2] **Alhadji Malloum** [ID],[3,4] **Charné Bornman** [ID],[2] **Christian Osagie** [ID],[5] **Leili Mohammadi** [ID],[6] and **Chinenye Adaobi Igwegbe** [ID][7]

[1]*Department of Environmental Health Engineering, Faculty of Medical Sciences, Tarbiat Modares University, Tehran, Iran*
[2]*Department of Genetics, Faculty of Natural and Agricultural Sciences, University of the Free State, Bloemfontein 9300, South Africa*
[3]*Department of Physics, Faculty of Science, University of Maroua, P.O. BOX 46, Maroua, Cameroon*
[4]*Department of Chemistry, University of the Free State, P.O. BOX 339, Bloemfontein 9300, South Africa*
[5]*Chair of Stochastics and its Applications, Brandenburg University of Technology, Cottbus, Senftenberg, Germany*
[6]*PhD of Environmental Health, Infectious Diseases and Tropical Medicine Research Center, Research Institute of Cellular and Molecular Sciences in Infectious Diseases, Zahedan University of Medical Sciences, Zahedan 98167-43463, Iran*
[7]*Department of Chemical Engineering, Nnamdi Azikiwe University, P. M. B. 5025, Awka, Nigeria*

Correspondence should be addressed to Chinenye Adaobi Igwegbe; ca.igwegbe@unizik.edu.ng

In order to assess the interactions between process factors, the experiments involving the liquid-phase adsorption of cephalexin (CEX) onto silicon-coated iron nanoparticles ($Fe_3O_4@SIO_2$) were designed using the Box-Behnken Design-Response surface methodology (BBD-RSM). Optimal circumstances were used to investigate the synergistic influence on the process's efficiency. In addition, the data was used to test and fit an artificial neural network (ANN) model. Molecular-level DFT calculations on the CEX molecule were carried out. The PW6B95D3/Def2-TZVP level of theory was used to build DFT-based descriptors for the CEX molecule. At 25°C, pH 5.83, 37.67 min, a dosage of 0.8 g $Fe_3O_4@SIO_2$ and 118.01 mg/L CEX, the removal efficiency achieved a maximum of 99.01 percent. For example, we found that OH — O, NH — O, CH — O hydrogen bonds, NH — π, OH — π, CH — π interactions as well as dipole-dipole interactions between CEX and the nanoparticles could all be used to connect the CEX and the nanoparticles. There is a strong correlation between the output and target values acquired by BBD-RSM and ANN fits. $Fe_3O_4@SIO_2$ proved to be an excellent tool for eliminating CEX.

1. Introduction

Antibiotic residues on the environment have been increasingly controversial in recent years. As a result, antibiotic depletion control has been explored extensively [1]. The development of antibiotic resistance is a big worry, even though medications are unlikely to have an immediate negative effect on aquatic microbes [2]. Antibiotic Cephalexin (CEX), which belongs to the penicillin group, is used in medicine and veterinary medicine to treat gastrointestinal and bacterial infections of the intestines and urinary tract [3].

One of the most widely used antibiotics is the beta-lactam family, which includes the molecule CEX [4, 5]. More serious side effects include limited biological decomposition capacity, high toxicity, carcinogenic, mutagenic, mutagenic effects, DNA and lymphocytes being damaged, allergic responses being increased, and the development of medication resistance [6]. Because of their complicated structure and limited biodegradability, the degradation of these substances is seen as a significant environmental concern [7].

Cephalexin (CEX) is an antibiotic that comes from the cephalosporin family and is widely regarded as the second-

most consumed group of antibiotics globally [8]. According to research evidence, it is known to be used as a treatment method normally to treat respiratory and urinary infections [9]. However, the discharge of contaminated water from pharmaceutical facilities, hospitals, homes, and agro-industrial facilities containing pharmaceuticals such as CEX into the environment can have adverse impacts on human health, increase antibiotic resistance, and inhibit the growth of algae and beneficial microorganisms in the environment [10]. Furthermore, the removal of cephalexin from effluents has not been fully studied. Adel et al. [11] worked on the removal of cephalexin antibiotic and heavy metals from pharmaceutical effluents using Bacillus subtilis strain. The removal of cephalexin from effluents by activated carbon prepared from alligator weed was studied by Miao et al. [12]. Furthermore, Miao et al. [12] studied the removal of cephalexin and erythromycin antibiotics and their resistance genes, by microalgae-bacteria consortium from wastewater treatment plant secondary effluents. In their findings, cephalexin and erythromycin had a removal efficiency of 96.54% and 92.38%, respectively. According to Miao et al. [12], cephalexin has been observed to be flowing out of hospital wastewaters, effluents, and wastewater treatment plants at mg L^{-1} levels. In the light of the above, it becomes imperative to develop and deploy new methods to effectively remove these contaminants from aqueous solutions using sustainable technologies under favorable economic conditions. Consequently, standard physicochemical and biological treatments can only breakdown a limited number of these compounds [13]. Reverse osmosis, ozonation, and other sophisticated treatment procedures can remove antibiotics from wastewater; however, these technologies may not be cost-effective, energy-efficient, operational, or ecologically justifiable [14, 15]. As a result, scientists are always searching for new approaches that are more effective, less expensive, and less harmful to the environment. Antibiotics, for example, are well-suited for elimination by adsorption [16]. Adsorption is a well-known approach for removing antibiotics that is both effective and ecologically safe, based on past research.

Imaging, sensing, targeted medicine administration, gene transfer systems, and artificial implants are all examples of how nanotechnology is being applied in medical research today [17, 18]. With these uses, nanotechnology can be beneficial to human health care, and it can be hoped that it could lead to breakthrough advancements in fields such as medicine, communication, genomics, and robotics [19]. Fe$_3$O$_4$@SiO$_2$ magnetite nanoparticles have been the primary focus of CEX adsorption. It is difficult to extract, process, and investigate uncoated magnetite nanoparticles since they agglomerate easily and have limited usefulness. As a result of this, we have recently reported on the electrochemical production of magnetite nanoparticles without the need of any organic solvent or surfactant [20].

The number of experiments to be conducted has been the subject of several theories and methodologies over the last few decades. Using statistical and mathematical methods, the response surface methodology (RSM) examines the influence of several independent variables [21]. There are various benefits to using the Box Behnken design
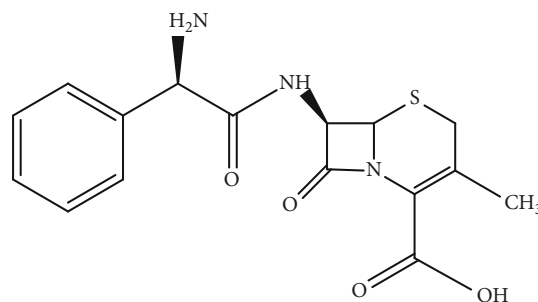

FIGURE 1: The chemical structure of CEX.

approach (a sort of RSM), including a statistical model that describes the process as exactly as possible while decreasing the number of test stages, time, cost, and material consumption [22]. Due to its ability to apply learning methods to discover input–output relationships for complex, nonlinear dynamic systems, artificial neural networks (ANNs) are increasingly being used as prediction tools in a variety of industries, including engineering [23].

As a result of this, the researchers conducted a study on the removal of CEX from an aqueous medium using silica-modified iron nanoparticles (Fe$_3$O$_4$@SiO$_2$). CEX antibiotics were also shown to have a wide range of efficacious factors ranging from contact time to temperature to dose. We used response surface methodology (RSM) in our research to better understand how different processes interact with one another and how to improve adsorption efficiency. Tested/fitted for the data were the artificial neural network (ANN) models CEX molecules and Fe$_3$O$_4$@SiO$_2$ were also studied using density functional theory in a computer investigation of the interaction/mechanism (DFT). In order to get a better knowledge of the CEX adsorption, the DFT was also employed to determine the chemical potential (μ), chemical hardness (η), flexibility (ζ), ionization potential (IP), electrophilicity index (ω), and electronic affinity (EA).

2. Materials and Methods

2.1. Materials. Cephalexin-CEX (C$_{16}$H$_{17}$N$_3$O$_4$S, 347.39 g/mol, 99.6%) were supplied by Sigma-Aldrich USA. The following diagram depicts the molecular structure of CEX (Figure 1). All solutions and buffers were prepared using distilled water. Citric acid and citrate acid were utilized to make a citrate buffer with a certain pH. The Thermo Scientific GENESYS 180 UV-visible spectrophotometer was used to obtain the concentration of CEX at 263 nm wavelength.

2.2. Synthesis of Fe$_3$O$_4$ Nanoparticles. The nanoparticles were produced using the chemical precipitation process. A 100-milliliter flask of dehydrated water with nitrogen gas, 4.5 g of FeCl$_3$.6H$_2$O and 2.78 g of FeCl$_2$.4H$_2$O is stirred constantly. This was achieved by adding ammonia solution (25 percent) and letting it sit until the solution became black. 30 minutes of stirring and heating to 80°C resulted in a precipitate that had developed. It was rinsed three times with ionized water, then twice with ethanol, after the precipitate produced during the heating process. The magnetic

nanoparticles (Fe_3O_4) were finally isolated from the magnetic solution by using a magnet.

2.3. Coated Iron Nanoparticles with Silica ($Fe_3O_4@SIO_2$).
Using the sol-gel process, silica was used to coat the nanoparticles. A solution comprising 150 mL ethanol, 2 mL water and 4 mM tetraethyl orthosilicate (TEOS) was added to the previous step's nanoparticles after they had been washed and dried. After 30 minutes of stirring, it was cleaned five times with ethanol before being dried. Drying and powder production of coated nanoparticles were carried out in a laboratory setting at room temperature.

2.4. Characterization of the Fe_3O_4 and $Fe_3O_4@SIO_2$.
The $Fe_3O_4@SIO_2$ and Fe_3O_4 morphological structures were examined using a LEO instrument, model 1455VP scanning electron microscopy (SEM). Experimenters employed Fourier-transform infrared spectroscopy to recognize the chemical groups contained in the Fe_3O_4 and $Fe_3O_4@SIO_2$ samples.

2.5. Batch Treatment Study.
As part of each experiment, 10 milliliters of the CEX antibiotic solution were in contact with $Fe_3O_4@SIO_2$ for a predetermined time duration at a predetermined temperature and pH. After reactions, 0.5 cc of samples were taken and filtered through a 0.22-micron filter. UV-Vis' spectrophotometer was used to quantify the antibiotic residue in the solution, and Equation (1) was used to compute the elimination % of CEX [24]:

$$\%R = \frac{(C_0 - C_f)}{C_0} 100, \quad (1)$$

where C_f and C_0 are the final and initial concentrations in ppm, respectively.

2.6. Experimental Design and Statistical Analysis.
An RSM of Design expert version 8.0.7.1 software, USA, was utilized to create 54-run experiments that included 8 axial and 16 factorial point locations as well as 6 replicates at the center points (Table 1) which included the dependent factors including pH, time, dose, and CEX concentration. In this investigation, the independent variables were coded in accordance with Equation (2):

$$Xi = \frac{(X_i - X_0)}{\Delta X} \times 100, \quad (2)$$

where X_0 is the value of X_i at the center point, X_i is the coded independent variable, and Δx is the step change value. The second-order polynomial model was used to explain the process (Equation (3)):

$$Y = \beta_0 + \sum_{i=1}^{k} \beta_i x_i + \sum_{i=1}^{k} \beta_{ii} x_i^2 + \sum_{i=1}^{k-1} \sum_{j}^{k} \beta_{ij} x_i x_j + \Sigma, \quad (3)$$

where Y is the predicted response, $x_i, x_j, \cdots, x_k$ are the input variables, which affects the response Y; $x_{2i}, x_{2j}, \cdots, x_{2k}$ are the square effects, β_0 is the intercept term, $x_i x_j$,

TABLE 1: Predicted and experimental values for CEX by $Fe_3O_4@SIO_2$.

Run	A pH	B Time (min)	C Dosage (g/L)	D C_0 (mg/L)
1	11	15	1	150
2	7	47.5	0.75	150
3	11	80	0.5	150
4	7	47.5	0.75	100
5	7	47.5	0.75	100
6	11	80	1	50
7	7	47.5	0.75	100
8	11	15	0.75	50
9	7	47.5	0.5	100
10	7	47.5	0.75	100
11	3	80	1	50
12	7	80	0.75	50
13	11	15	0.5	150
14	3	15	0.5	150
15	11	80	1	150
16	3	47.5	0.75	100
17	7	47.5	0.75	100
18	3	15	1	150
19	3	15	0.5	50
20	7	15	0.75	100
21	7	47.5	1	100
22	3	80	0.5	50
23	11	80	0.5	50
24	11	15	1	50
25	11	47.5	0.75	100
26	3	80	0.5	150
27	7	47.5	0.75	100
28	3	15	1	50
29	3	80	1	150
30	7	47.5	0.75	50

$x_j x_k$, and $x_i x_k$ are the interaction effects, $\beta_i (i = 1, 2, \cdots, k)$ is the linear effect, $\beta_{ii} (i = 1, 2, \cdots, k)$ is the squared effect, $\beta_{ij} (j = 1, 2, \cdots, k)$ is the interaction effect, and $\sum$ is the random error [25].

The experimental levels tried for CEX onto $Fe_3O_4@SIO_2$ particles are indicated in Table 2. The empirical second-order polynomial regression model (Equation (3)) was used to fit the experimental data. The experiments were run following the method mentioned in Section 2.5 following the variables' conditions in Table 1.

2.7. Computational Methodology.
To get further understanding on CEX adsorption, a computer analysis of the CEX molecule was conducted. The computations were carried out using the density functional theory (DFT) functional PW6B95D3 in conjunction with the Def2-TZVP basis set. The optimizations were carried out using the tight option

TABLE 2: Experimental levels tried for CEX onto $Fe_3O_4@SIO_2$ particles.

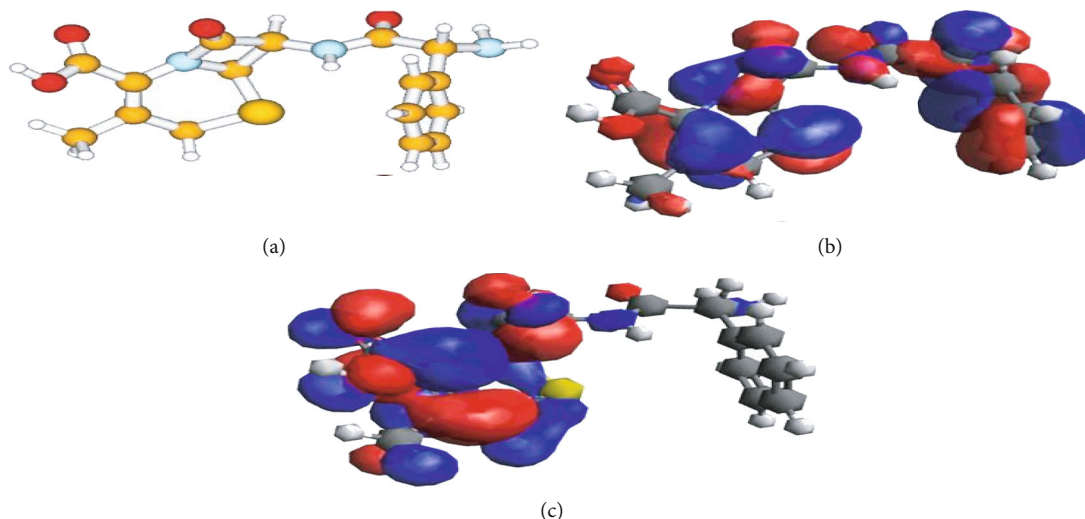| Factor	Independent variables	Unit	Range and level of actual and coded values		
			-1	0	+1
A (X_1)	Initial pH	—	3	7	11
B (X_2)	Time	min	15	47.5	80
C (X_3)	Dosage	g/L	0.5	0.75	1
D (X_4)	Concentration of CEX	mg/L	50	100	150

(a)

(b)

(c)

FIGURE 2: (a) Structure of CEX molecule as optimized at the PW6B95D3/Def2-TZVP level of theory. (b) HOMO; (c) LUMO of the CEX molecule.

TABLE 3: DFT-based descriptors of the CEX molecule as calculated at the PW6B95D3/Def2-TZVP level of theory. The energy unit used in the table is eV.

E_{HOMO}	E_{LUMO}	E_{gap}	η	ζ	μ	ω	IE	EA
-6.95	-1.37	5.57	2.79	0.36	-4.16	3.10	8.02	-0.46

selected for accuracy. We utilize the ultrafine grid for integrals because it is suggested for molecules with a large number of tetrahedral centers, for optimizing molecules with a large number of soft modes, and for calculating extremely low-frequency modes of systems. The energies of the orbitals were calculated, especially those of the highest occupied molecular orbital (HOMO) and lowest unoccupied molecular orbital (LUMO). The HOMO and LUMO energies were utilized to determine the chemical hardness (η), chemical potential (μ), flexibility (ζ), and electrophilicity index (ω) [26–28]:

$$\eta = -\frac{(E_{HOMO} + E_{LUMO})}{2},$$

$$\zeta = \frac{1}{\eta},$$

$$\mu = \frac{(E_{HOMO} + E_{LUMO})}{2},$$

$$\omega = \frac{\mu^2}{2\eta},$$

(4)

In addition, the ionization potential (IP) and the electronic affinity (EA) were calculated using the following formula [29, 30]:

$$IP = E^+ - E^0,$$

$$EA = E^- - E^0,$$

(5)

where E^0, E^+, and E^- represent the energies of neutral CEX, cationic, and anionic CEX molecules, respectively.

3. Result and Discussion

3.1. Computational Analysis. As can be seen in Figure 2(a), the CEX molecule's structure has been optimized to the PW6B95D3/Def2-TZVP level of theoretical theory. Additionally, we have shown in Figure 2 the structural distribution of the Homo and Lumo, as well as the optimization of the structure (Figures 2(b) and 2(c), respectively). Table 3 lists the CEX molecule's computed DFT-based characteristics.

There appears to be a consistent distribution of the HOMO across the structure. CEX will be attracted to the
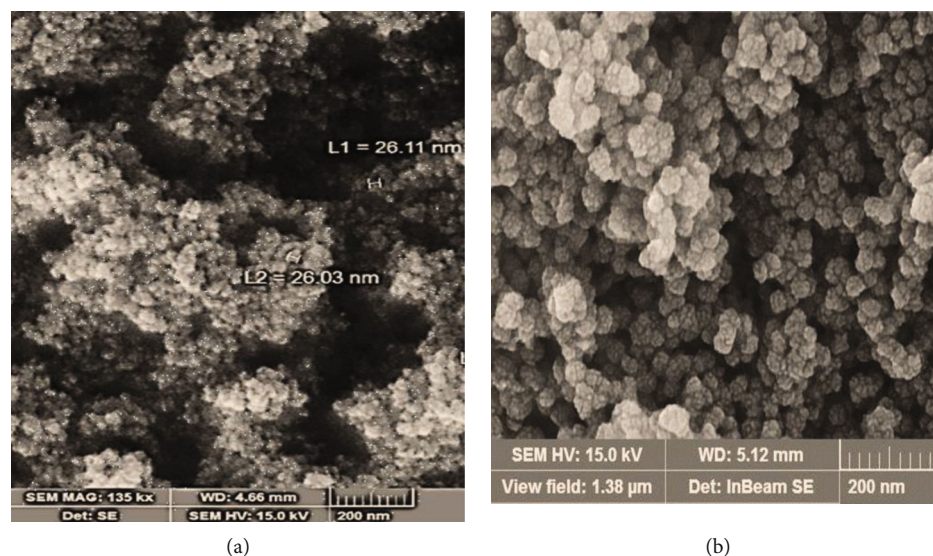
FIGURE 3: SEM micrograph of Fe_3O_4 (a) and $Fe_3O_4@SIO_2$ (b).

nanoparticles through the various -NH, -OH, and -CH groups of the nanoparticles molecule's molecule, as seen in this diagram. The LUMO is also found on the other side of the molecule, but not in any of the benzenoic rings. The CEX molecule acts as a proton donor for the nanoparticles, making it possible to interact with them. Hydrogen bonds, NH —- O, OH —- O, CH —- O, NH — π, OH — π, CH — π interactions as well as dipole-dipole interactions are all demonstrated in the HOMO and LUMO experiments as possible mechanisms for mediating interactions between the CEX molecule and nanoparticles. Because of this, it is been discovered that nanoparticle molecules may strongly adsorb the CEX molecule via the various interactions indicated above in studies of its HOMO and LUMO. And the molecule's moderate chemical hardness value (2.79) eV confirms that it is highly reactive.

Computational studies were conducted in this work to give an explanation for the interactions between the CEX molecule and iron nanoparticles covered with a layer of iron oxide. A thorough description of these interactions would include all the molecules involved and compute the interaction free energy at the relevant experimental temperature. Because the experiment is being replicated, it is necessary to make computations in solution. Molecular dynamics simulations or a combination of quantum mechanics and molecular mechanics molecular dynamics simulations are unable to handle the complexity of these computations. Our calculations have been restricted to the analysis of the CEX molecule by offering certain DFT-based descriptors that might explain the probable interactions, due to tractability and affordability.

3.2. Characteristics of Nanoparticles.
Particle morphology, shape, and size may be determined using scanning electron microscopy (SEM) techniques [31, 32]. Images of Fe_3O_4 and $Fe_3O_4@SIO_2$ particles are revealed in Figure 3. Compared to the Fe_3O_4, the $Fe_3O_4@SIO_2$ particles seem rounder and more uniform in shape in SEM images. Cheng et al. [33]

also obtained round $Fe_3O_4@SIO_2$ particles from their study. Figure 4 shows the FTIR data for the Fe_3O_4 and $Fe_3O_4@SIO_2$ particles. Si-O-H and Si-O-Si have been detected in both spectra after silicon has been applied to $Fe_3O_4@SIO_2$ particles, confirming that silicon has been applied to the Fe_3O_4 particles. Both particles shared functional groups including OH, Fe-O, and C=N. Similar result was observed by Du et al. [34] when FTIR analysis was done on both particles.

3.3. Model Fitting, Statistical Analysis, and Optimization.
According to Table 4, the adsorption experiments were executed. Design expert 8.0.7.1 software, USA, was used to evaluate and interpret the produced data. As shown in Table 4, the quadratic model outperforms all other models (interactive, linear, and cubic) except the cubic model in terms of R^2, adjusted R^2, and anticipated R^2. Because the cubic model aliased, it cannot be utilized to model the data. When there are not enough experiments to evaluate all of the models equally, we have an aliased model [35]. To select the best models, we used the sequential model sum of squares and model summary statistics (Table 5). While 2FI is substantial, it is not aliased by quadratics. The quadratic model was recommended by the program because it maximizes the adjusted R^2 and predicted R^2 values. A single experimental run's response results were quite close to the projected values (Figure 5 and Table 6).

Response surface quadratic model ANOVA findings are shown in Table 7. Analyzing ANOVA results helps to determine if the quadratic model produced is statistically appropriate for describing processes like CEX in this study's study range. An F value of 119.99 indicates that the model is statistically significant. An F value this great in a model has a noise probability of less than one-hundredth of one percent. Model terms that have p values less than 0.05 are considered significant [36]. A, C, D, AC, A^2, C^2, and D^2 are the significant model terms in this example. The model terms with p values larger than 0.10 are not significant. The likelihood of rejecting a null hypothesis is known as
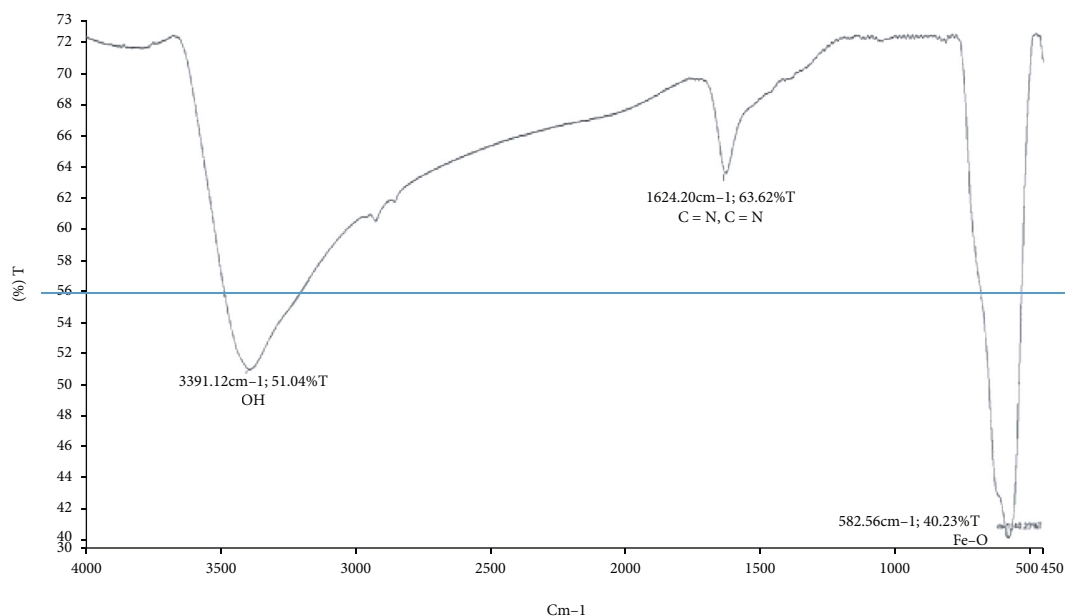
(a)
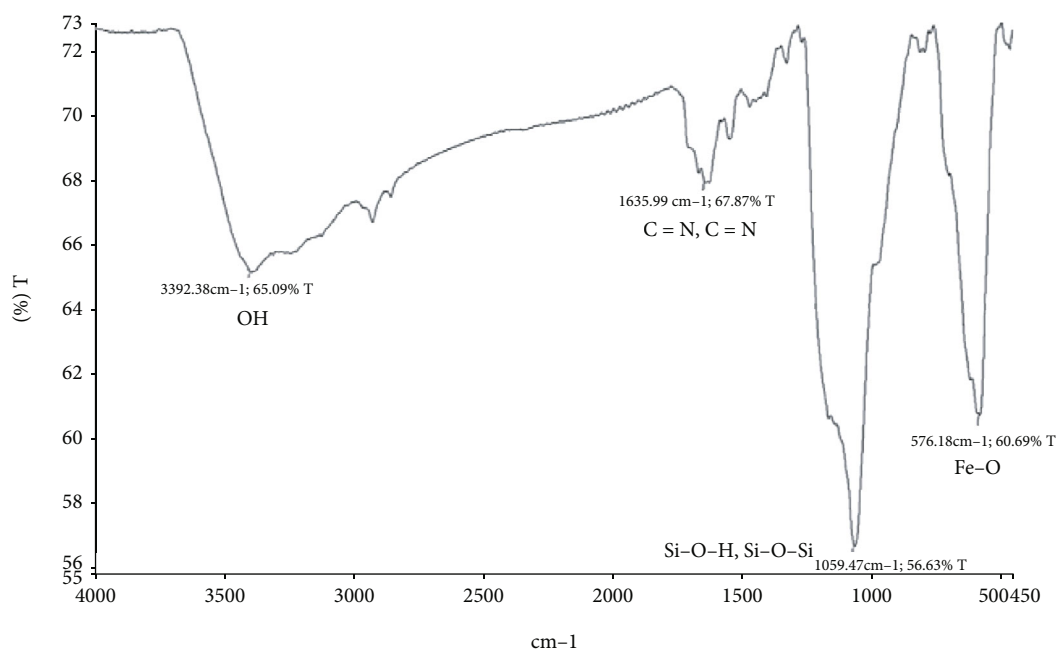
(b)

FIGURE 4: FTIR spectra of (a) Fe_3O_4 and (b) $Fe_3O_4@SIO$.

TABLE 4: Fit summary of the analysis.

Linear	0.0001	<0.0001	0.5266	0.4172	
2FI	0.9492	<0.0001	0.4242	-0.3827	
Quadratic	<0.0001	<0.0001	0.9829	0.9558	Suggested
Cubic	0.0736	<0.0001	0.9921	0.7218	Aliased

the p value. The more important the individual coefficients and the more appropriate the model are, the higher the Fisher's F value [37]. Noise has an 11.98 percent likelihood of causing such a severe lack of fit F value. It is fine if there

is a small amount of mismatch. Because this model does not match the experimental data and because the independent process factors affect the response in an important way, it has a p value of larger than 0.05. It is the coefficient of a given process variable and the two combined variables that indicate how much influence a variable has and how it interacts with other variables, respectively. The expected R^2 (0.9558) and the amended R^2 (0.9829) are reasonably close. The great degree of connection between the anticipated and experimental responses is validated by the R^2 (coefficient of determination), which is 0.9911. The model's validity is shown by the closeness of these values to unity

TABLE 5: Model summary statistics and sequential model sum of squares for CEX by nanoparticles.

(a)

Sequential model sum of squares						
Mean vs. total	2.842E+05	1	2.842E+05			
Linear vs. mean	65.07	4	16.27	9.06	0.0001	
2FI vs. linear	3.39	6	0.5657	0.2592	0.9492	
Quadratic vs. 2FI	40.50	4	10.12	156.09	<0.0001	Suggested
Cubic vs. quadratic	0.7620	8	0.0953	3.16	0.0736	Aliased
Residual	0.2109	7	0.0301			
Total	2.843E+05	30	9475.71			

(b)

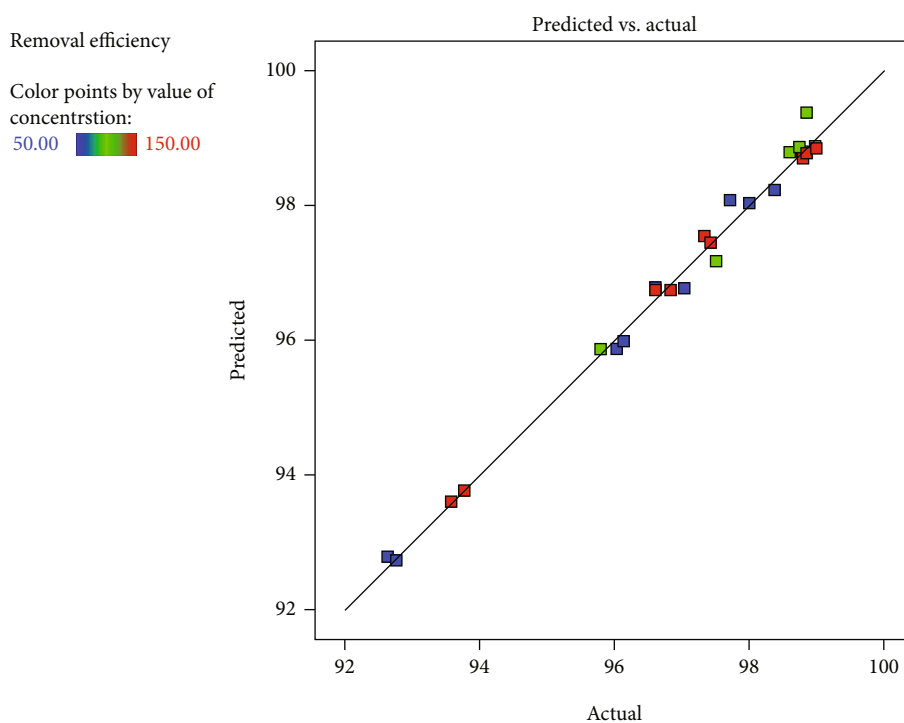| Model summary statistics						
Linear	1.34	0.5919	0.5266	0.4172	64.07	
2FI	1.48	0.6228	0.4242	-0.3827	152.00	
Quadratic	0.2547	0.9911	0.9829	0.9558	4.86	Suggested
Cubic	0.1736	0.9981	0.9921	0.7218	30.58	Aliased
Linear	1.34	0.5919	0.5266	0.4172	64.07	

FIGURE 5: The plot of the predicted values versus the observed values of CEX adsorption on $Fe_3O_4@SIO_2$.

[38]. Appropriate accuracy is used to determine the signal-to-noise ratio, which should be greater than 4. The adequate precision ratio of 36.9042 specifies an adequate signal. The design space may be navigated using this concept.

The model conveying the response (CEX removal efficiency) and process factors is shown as Equation (6):

$$E = 98.88 - 1.50A - 0.00537B - 1.10C + 0.38D + 0.017AB - 0.45AC + 0.052AD + 0.044BC. \tag{6}$$

In this regard: (A) pH, (B) reaction time (minutes), (C) dosage, (D) CEX concentration (mg/L).

TABLE 6: Predicted and experimental values for CEX by $Fe_3O_4@SIO_2$.

Run	A pH	B Time (min)	C Dosage (g/L)	D C_0 (mg/L)	Experimental R (%)	Predicted R (%)
1	11	15	1	150	93.58	93.62
2	7	47.5	0.75	150	99	98.85
3	11	80	0.5	150	96.84	96.74
4	7	47.5	0.75	100	98.98	98.88
5	7	47.5	0.75	100	98.97	98.88
6	11	80	1	50	92.64	92.79
7	7	47.5	0.75	100	98.99	98.88
8	11	15	0.75	50	96.14	96
9	7	47.5	0.5	100	98.85	99.38
10	7	47.5	0.75	100	99.01	98.88
11	3	80	1	50	97.04	96.77
12	7	80	0.75	50	98.60	98.8
13	11	15	0.5	150	96.62	96.75
14	3	15	0.5	150	98.86	98.78
15	11	80	1	150	93.77	93.78
16	3	47.5	0.75	100	98.75	98.88
17	7	47.5	0.75	100	99	98.88
18	3	15	1	150	97.43	97.45
19	3	15	0.5	50	98.37	98.23
20	7	15	0.75	100	98.79	98.81
21	7	47.5	1	100	97.50	97.18
22	3	80	0.5	50	98	98.04
23	11	80	0.5	50	96.04	95.88
24	11	15	1	50	92.77	92.74
25	11	47.5	0.75	100	95.79	95.88
26	3	80	0.5	150	98.80	98.7
27	7	47.5	0.75	100	98.97	98.88
28	3	15	1	50	96.61	96.78
29	3	80	1	150	97.34	97.55
30	7	47.5	0.75	50	97.71	98.08

To accurately forecast the output response, the above model equation's unimportant terms can be deleted (Grenni et al. 2018). CEX concentration, however, has a synergetic effect on the adsorption of CEX. Also, the interaction between pH and time has a synergetic effect on the process as well as the interaction between pH and CEX concentration. Solution pH, reaction duration, dose, temperature, and the interaction between pH and dosage have an antagonistic effect on CEX oxidation looking at the signs in Equation (6). The higher F value for pH (Table 7) shows that the pH has the greatest influence on the adsorption of CEX using $Fe_3O_4@SIO_2$ particles.

Figure 6 depicts the normal percent probability vs. internally studentized residuals (Figure 6), which show that there was little divergence from the norm. There is no need to alter the data because the graphical points follow a straight line [39]. Independent process factors are examined for their combined influence on a response using the RSM statistical approach [40]. Response surface plots of any two process factors versus any two additional process variables were used to analyze the interaction of the process variables and their associated impacts on CEX adsorption.

The 3D surface plots of the relation between the process variables and their associated output responses are shown in Figures 7(a)–7(f). The adsorbing material's functional groups and the pH of the solution play an important role in the adsorption process [32, 41]. The enzyme ionizes the amino acids in the molecule and alters their nature when the pH is acidic, resulting in the placement of the hydrogen ion on the nitrogen atom of the protein molecule [36, 38]. There are hydroxide ions attached to reactive groups at alkaline pHs, which have positive charges and prevent electrons from being transferred from the substrate to active sites of lacasses [42]. In somewhat acidic circumstances, the pH range of 4-6 is optimal for most fungal laccase oxidation [36, 38]. Increasing or reducing the pH of this value has the greatest effect on the elimination of CEX in both free and dose methods. There was also less oxidation. In contrast

TABLE 7: ANOVA for the response surface quadratic model of CEX adsorption on $Fe_3O_4@SIO_2$.

| Source	Sum of squares	df	Mean square	F value	p value Prob> F
Model	108.96	14	7.78	119.99	<0.0001
A-pH	40.57	1	40.57	625.46	<0.0001
B-time	5.191E-004	1	5.191E-004	8.003E-003	0.9299
C-dosage	21.84	1	21.84	336.68	<0.0001
D-concentration	2.66	1	2.66	40.97	<0.0001
AB	4.444E-003	1	4.444E-003	0.069	0.7971
AC	3.29	1	3.29	50.69	<0.0001
AD	0.043	1	0.043	0.66	0.4298
BC	0.031	1	0.031	0.47	0.5025
BD	0.013	1	0.013	0.20	0.6627
CD	0.015	1	0.015	0.23	0.6352
A^2	5.83	1	5.83	89.87	<0.0001
B^2	0.016	1	0.016	0.25	0.6277
C^2	0.92	1	0.92	14.22	0.0018
D^2	0.45	1	0.45	6.93	0.0188
Residual	0.97	15	0.065		
Lack of fit	0.97	10	0.097	374.25	<0.0001
Pure error	1.298E-003	5	2.596E-004		
Cor. total	109.93	29			
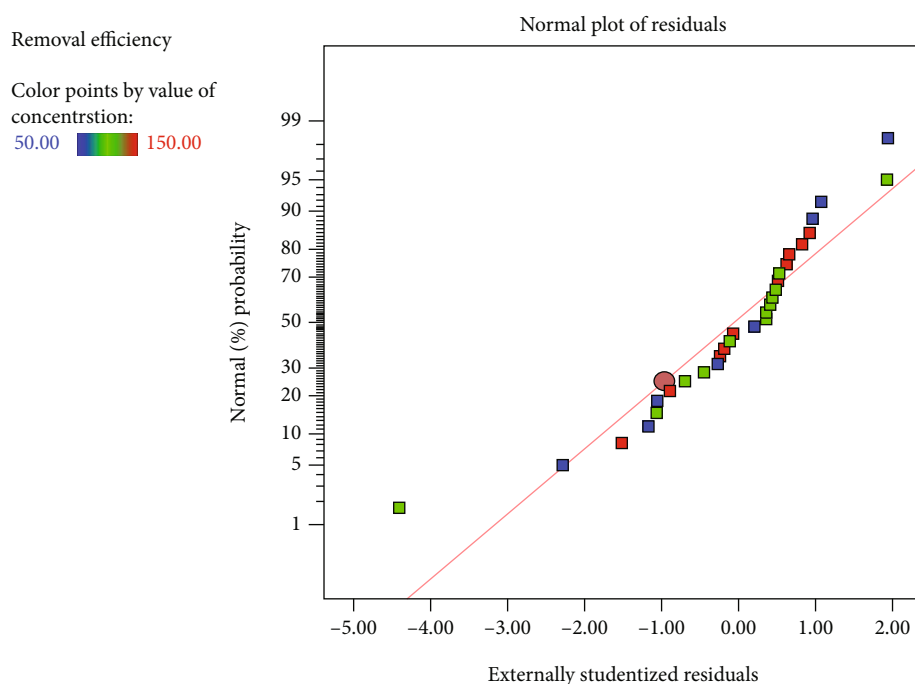
FIGURE 6: Normal probability plots of the residuals for CEX adsorption on $Fe_3O_4@SIO_2$.

to the efficiency decline caused by nanoparticles, this decrease happens in the adsorption process and has a lesser slope. Figures 7(a) and 7(b) demonstrates that the reaction time and elimination of CEX is maximum and occurs in 60 minutes at pH 3.

Increasing the contact period from 15 to 60 minutes significantly improves the effectiveness of antibiotic CEX removal via adsorption, since nanoparticles have a direct relationship with removal efficacy. The maximum removal efficiency is achieved in 60 minutes for both procedures.
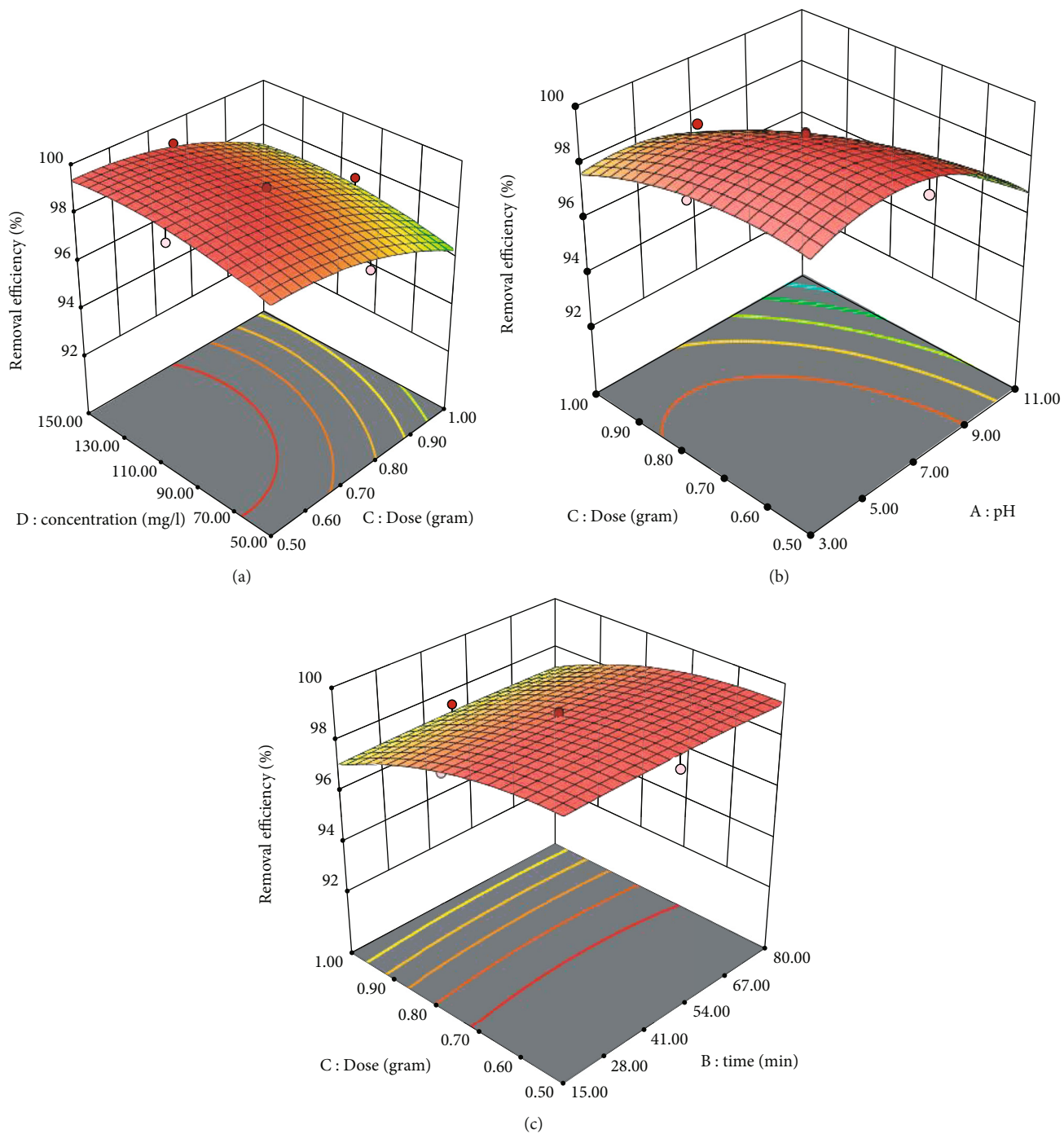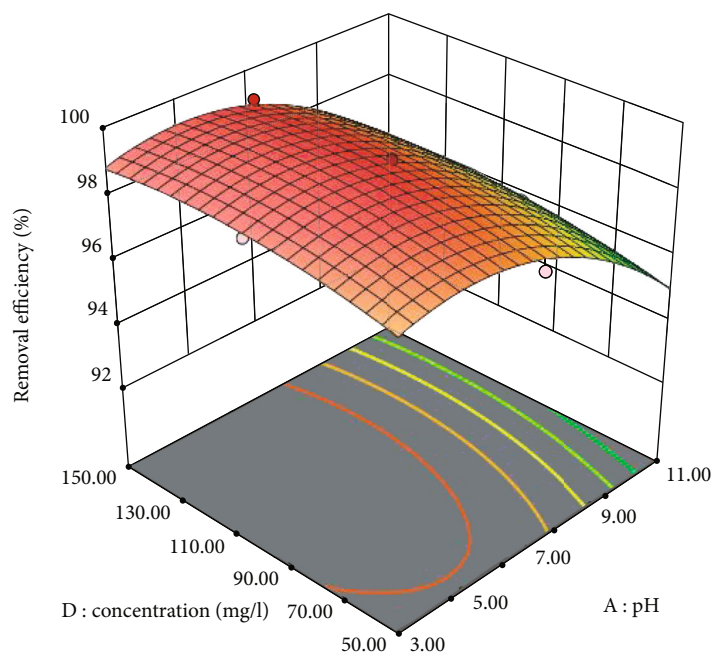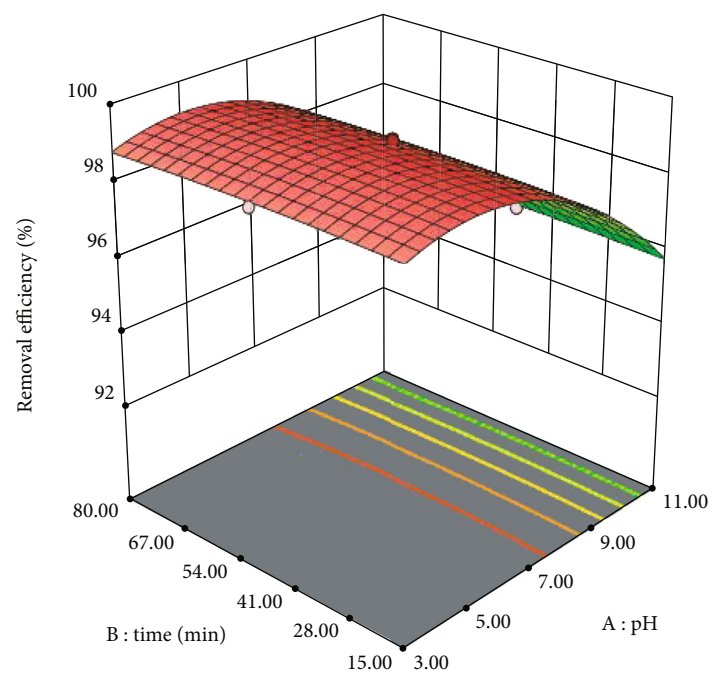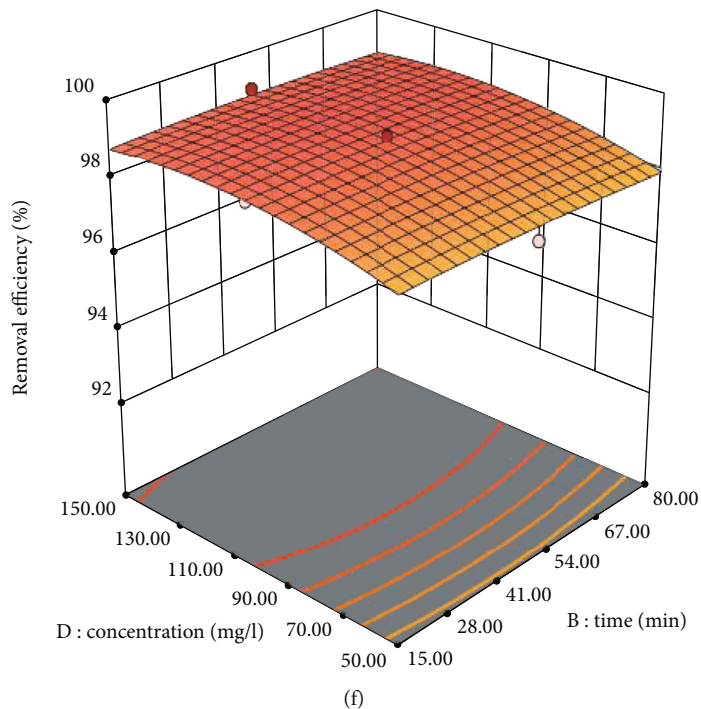
(a)

(b)

(c)

Figure 7: Continued.

(d)

(e)

FIGURE 7: Continued.

(f)

FIGURE 7: 3D surface plots of the interactive effect of CEX on $Fe_3O_4@SIO_2$.
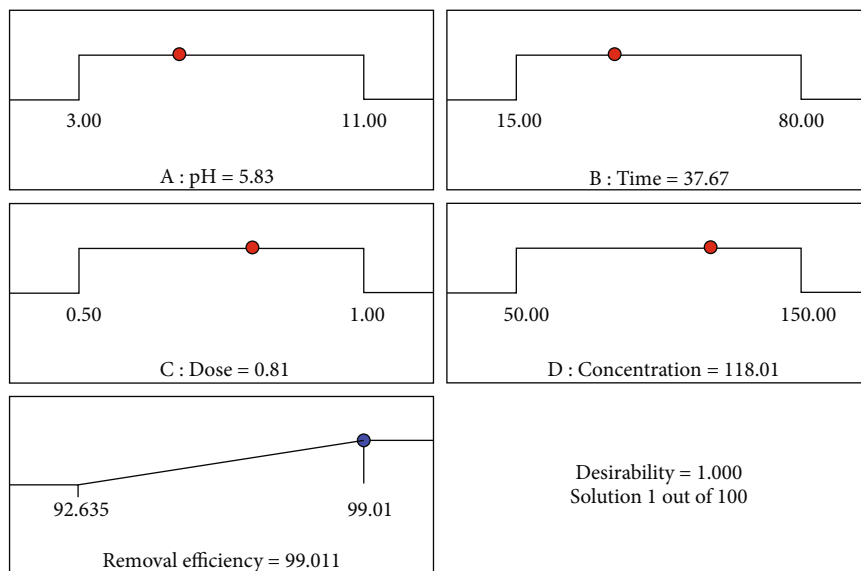

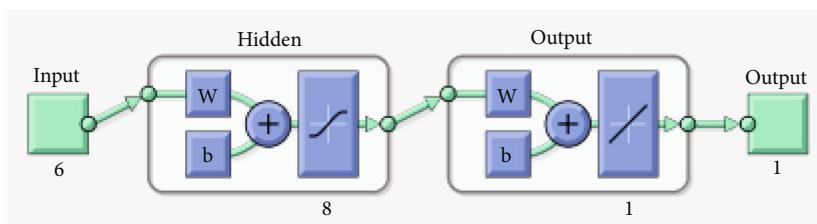FIGURE 8: Desirability effect for the CEX-$Fe_3O_4@SIO_2$ process.

FIGURE 9: The proposed neural network architecture.

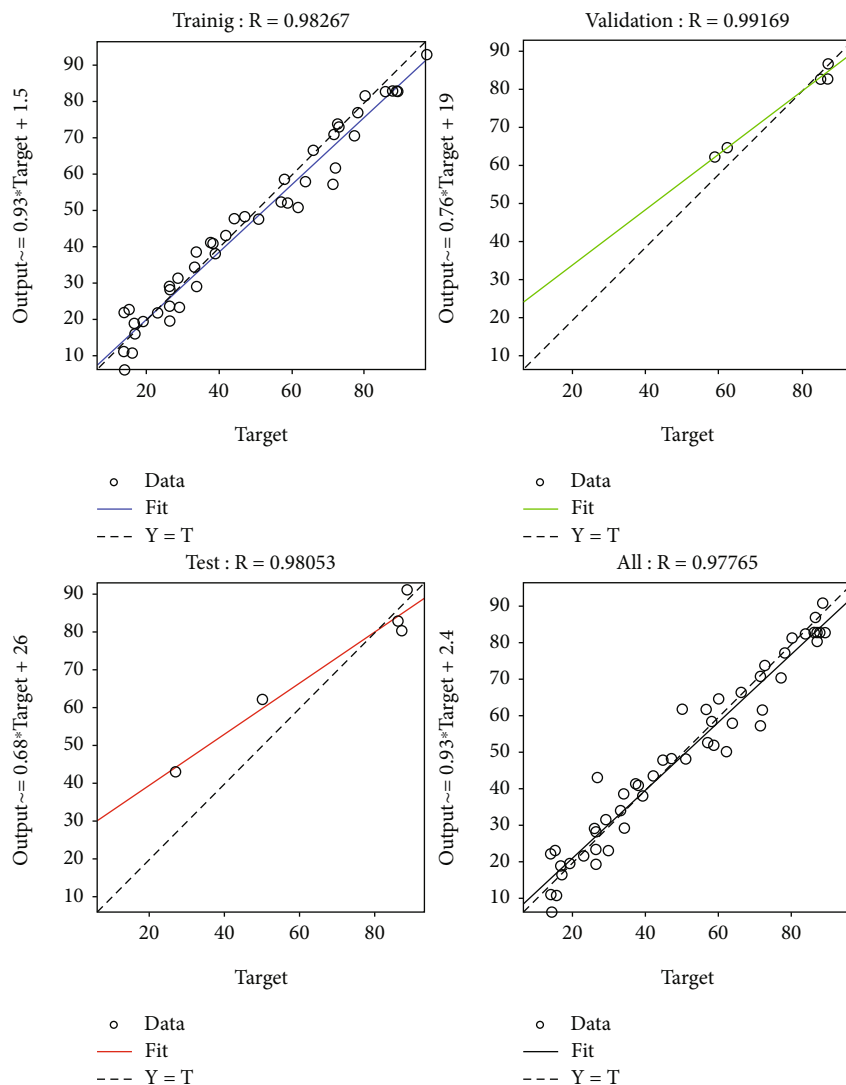FIGURE 10: Regression plot for CEX onto $Fe_3O_4@SIO_2$.

Figures 7(a)–7(c) show the effect of $Fe_3O_4@SIO_2$ dose on the efficacy of eradicating CEX antibiotics in the range of 0.5 and 1 g during nanoparticle adsorption. CEX removal was increased with elevated $Fe_3O_4@SIO_2$ dose; similar observation was made when zeolite coated with magnetic Fe3O4 nanoparticles was used for CEX removal [43]. By raising the CEX concentration from 50 mg/L to 150 mg/L, the clearance rate was significantly decreased (Figures 7(a), 7(d), and 7(f)). Increasing the concentration led to more saturation of the $Fe_3O_4@SIO_2$; similar trend was observed in past study where activated carbon derived from pomegranate peel was used [44]; the same authors observed an optimum pH of 5. In addition, the percentage of deletions rose as the interaction duration grew from 15 minutes to 60 minutes (Figures 7(c), 7(e), and 7(f)). At 25°C, pH 5.83, 37.67 min, 0.8 g $Fe_3O_4@SIO_2$, and 118.01 mg/L CEX, the removal efficiency achieved a maximum of 99.01 percent, according to numerical optimization data (Figure 8). $Fe_3O_4@SIO_2$ was shown to remove CEX with an efficiency of 98.9 ± 0.73% in tests conducted at these locations.

3.4. Artificial Neural Network (ANN) Modeling. Using a tanh-sigmoid activated hidden neuron and a linearly activated output neuron in a two-layered feed-forward network, the parameter was estimated. Levenberg-Marquardt backpropagation was used to train the network. Shown below is an example of how a neural network may look (Figure 9). An input into a neuron with a value between +1 and -infinity may be squashed to produce an output of -1 to 1 using the tanh-sigmoid activation function. Tanh-sigmoid activation function is a mathematical representation of this function.

$$g(z) = \frac{2}{1 + e^{-2Z}} - 1, \tag{7}$$

where z is the vector product of the neuron weight transposed (Θ^T) ($z = \Theta^T x$) and the input value (x); $g(z)$ is the tanh-sigmoid function. This transfer function is commonly used in backpropagation networks to determine the output [45], in part because it is differentiable.
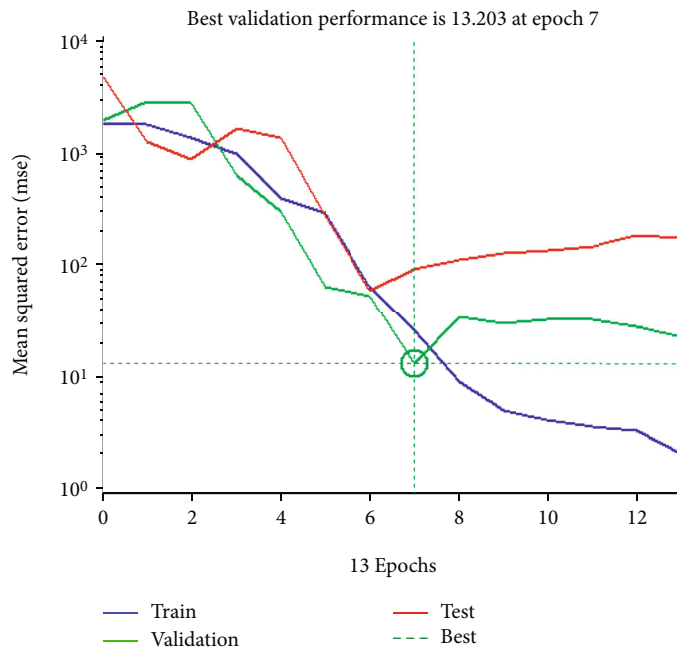
Best validation performance is 13.203 at epoch 7

FIGURE 11: Performance plot for CEX onto $Fe_3O_4@SIO_2$.

The linear transfer function takes the input to the neuron (in this case output from the tanh-sigmoid hidden layer) and turns it into a continuous number. The linear activation function calculates the neuron's output by simply returning the value passed to it [46, 47]. Mathematically, the linear activation function is represented as.

$$a = \text{purelin}(n) = \text{purelin}(Wp + b) = Wp + b. \quad (8)$$

The cost (error) function is the function used to minimize the error between the output (result by the network) and the target [48]. Because parameter estimation is a multiple regression analysis problem that output continuous values. mean squared error cost function was used to train the network. The mean squared error cost function is given below:

$$J = \frac{1}{m} \sum_{i=1}^{m} (P(i) - y(i))^2, \quad (9)$$

where p is the model output of the training example and y is the reservoir response of the training example.

The procedures with which the network was trained can be summarized in the following steps:

(i) Import or read the training data (time and pressure data of the well test) from an excel data sheet to MATLAB as variables

(ii) Choose the training algorithm in this case the Levenberg-Marquardt backpropagation

(iii) Choose the number of neurons in this chase twenty (8).

(iv) Preprocess the input data to prevent outliers

(v) Divide the input data randomly into three parts for training, validating, and testing of the algorithm (in this case the division was made in the ratio of $80:10:10$) to prevent overfitting

(vi) Select the cost or error (in this case the mean square error) function to be minimized

(vii) Train the network to meet the goal (until the cost function is minimized and the variables converge).

Figure 10 shows how well the data were fitted to provide the coefficient of determination for the training, validation, and testing sets after 13 iterations. The total index of fitness is 0.9777, with a mean squared error of 31.44702. A suitable stopping point (Figure 11) was found at epoch 7 when the best validation performance of 13.203 was achieved. The R^2 values show that the output and the target values have a good connection [49–51]. This equation was utilized to estimate the ANN model values by plotting the validation outputs, Y against the targets, T (the experiment values) in Figure 11 and

$$Y = (0.76) T + (19). \quad (10)$$

4. Conclusion

Box-Behnken design-response surface (BBD-RSM) approach was used to examine the interactions between process factors on the liquid-phase adsorption of cephalexin (CEX) onto silicon-coated iron nanoparticles ($Fe_3O_4@SIO_2$). PW6B95D3/Def2-TZVP level of theory was used to calculate CEX's density functional theory- (DFT-) based descriptors. The elimination efficiency was found to be at its peak at 99.01 percent in the study. The elimination efficiency was found to be 99.01 percent at $25°C$, pH 5.83, 37.67 min,

dosage 0.8 g $Fe_3O_4@SIO_2$, and 118.01 mg/L CEX, with the highest concentration tested. A variety of interactions between the CEX molecule and the $Fe_3O_4@SIO_2$ might be established through OH — O, NH — O, CH — O hydrogen bonds, NH — π, OH — π, and CH — π interactions as well as dipole-dipole interactions. There is a strong correlation between the R^2 values produced from BBD-RSM and ANN fits and the output and target values. In general, the results of this study showed that the magnetic particles modified with silica has a good ability to remove CEX from aqueous media and can be considered as a suitable option to remove this contaminant.

Data Availability

No data were used to support this study.

Conflicts of Interest

There are no conflicts of interest declared by the authors.

Acknowledgments

References

[1] K. O. Iwuozor, T. A. Abdullahi, L. A. Ogunfowora et al., "Mitigation of levofloxacin from aqueous media by adsorption: a review," *Sustainable Water Resources Management*, vol. 7, no. 6, pp. 1–18, 2021.

[2] A. M. Banach, A. Mollazehi, and S. Ahmadi, "Survey on the removal of ciprofloxacin from aqueous solutions by nano-sono-catalytic process," *Desalination and Water Treatment*, vol. 136, pp. 207–211, 2018.

[3] R. Ding, Y. Chen, Q. Wang et al., "Recent advances in quantum dots-based biosensors for antibiotic detection," *Journal of Pharmaceutical Analysis*, 2021.

[4] T. Chaudhary, M. K. Chaudhary, B. D. Joshi, M. S. A. de Santana, and A. P. Ayala, "Spectroscopic (FT-IR, Raman) analysis and computational study on conformational geometry, AIM and biological activity of cephalexin from DFT and molecular docking approach," *Journal of Molecular Structure*, vol. 1240, article 130594, 2021.

[5] N. Devi, K. Rani, P. Kharb, and M. Prasad, "Herbal medicine for urinary tract infections with the blazing nanotechnology," *Journal of Nanoscience and Nanotechnology*, vol. 21, no. 6, pp. 3495–3512, 2021.

[6] C. A. Adeyanju, S. Ogunniyi, R. Selvasembian et al., "Recent advances on the aqueous phase adsorption of carbamazepine," in *ChemBioEng Reviews*, Wiley Online Library, 2022.

[7] N. Khoshnamvand, S. Ahmadi, and F. K. Mostafapour, "Kinetic and isotherm studies on ciprofloxacin an adsorption using magnesium oxide nanoparticles," *Journal of Applied Pharmaceutical Science*, vol. 7, no. 11, pp. 079–083, 2017.

[8] A. Watkinson, E. Murby, D. W. Kolpin, and S. Costanzo, "The occurrence of antibiotics in an urban watershed: from wastewater to drinking water," *Science of the Total Environment*, vol. 407, no. 8, pp. 2711–2723, 2009.

[9] A. Perea, R. E. Palma-Goyes, J. Vazquez-Arenas, I. Romero-Ibarra, C. Ostos, and R. A. Torres-Palma, "Efficient cephalexin degradation using active chlorine produced on ruthenium and iridium oxide anodes: role of bath composition, analysis of degradation pathways and degradation extent," *Science of the Total Environment*, vol. 648, pp. 377–387, 2019.

[10] Z. W. Zeng, X. F. Tan, Y. G. Liu et al., "Comprehensive adsorption studies of doxycycline and ciprofloxacin antibiotics by biochars prepared at different temperatures," *Frontiers in Chemistry*, vol. 6, p. 80, 2018.

[11] A. Adel, J. Lalung, A. Efaq, and N. Ismail, "Removal of cephalexin antibiotic and heavy metals from pharmaceutical effluents using Bacillus subtilis strain," *Expert Opinion on Environmental Biology Journal*, vol. 4, p. 2, 2015.

[12] M.-S. Miao, Q. Liu, L. Shu, Z. Wang, Y.-Z. Liu, and Q. Kong, "Removal of cephalexin from effluent by activated carbon prepared from alligator weed: kinetics, isotherms, and thermodynamic analyses," *Process Safety and Environmental Protection*, vol. 104, pp. 481–489, 2016.

[13] A. S. Oberoi, Y. Jia, H. Zhang, S. K. Khanal, and H. Lu, "Insights into the fate and removal of antibiotics in engineered biological treatment systems: a critical review," *Environmental Science & Technology*, vol. 53, no. 13, pp. 7234–7264, 2019.

[14] K.-J. Choi, S.-G. Kim, and S.-H. Kim, "Removal of antibiotics by coagulation and granular activated carbon filtration," *Journal of Hazardous Materials*, vol. 151, no. 1, pp. 38–43, 2008.

[15] L. J. Sweetman, L. J. Alcock, J. D. McArthur, E. M. Stewart, G. Triani, and S. F. Ralph, "Bacterial filtration using carbon nanotube/antibiotic buckypaper membranes," *Journal of Nanomaterials*, vol. 2013, Article ID 781212, 11 pages, 2013.

[16] R. Zein, L. Hevira, S. Fauzia, and J. O. Ighalo, "The improvement of indigo carmine dye adsorption by Terminalia catappa shell modified with broiler egg white," in *Biomass Conversion and Biorefinery*, pp. 1–18, Springer, 2022.

[17] K. Dulta, G. Koşarsoy Ağçeli, P. Chauhan, R. Jasrotia, P. Chauhan, and J. O. Ighalo, "Multifunctional CuO nanoparticles with enhanced photocatalytic dye degradation and antibacterial activity," *Sustainable Environment Research*, vol. 32, no. 1, pp. 1–15, 2022.

[18] L. A. Ogunfowora, K. O. Iwuozor, J. O. Ighalo, and C. A. Igwegbe, "Trends in the treatment of aquaculture effluents using nanotechnology," *Cleaner Materials*, vol. 2, article 100024, 2021.

[19] S. Ahmadi, M. Mesbah, C. A. Igwegbe et al., "Sono electrochemical synthesis of LaFeO3 nanoparticles for the removal of fluoride: optimization and modeling using RSM, ANN and GA tools," *Journal of Environmental Chemical Engineering*, vol. 9, no. 4, article 105320, 2021.

[20] S. Rahdar, S. Ahmadi, Z. Aramesh, and A. Rahdar, "Synthesis and efficiency evaluation Fe2O3@ SiO2 nanoparticle in acid blue 92 removal from aqueous solutions: equilibrium and kinetic studies," *Journal of Water and Wastewater Science and Engineering*, vol. 5, no. 1, pp. 23–32, 2020.

[21] D. Ozturk, T. Sahan, T. Bayram, and A. Erkus, "Application of response surface methodology (RSM) to optimize the adsorption conditions of cationic basic yellow 2 onto pumice samples as a new adsorbent," *Fresenius Environmental Bulletin*, vol. 26, pp. 3285–3292, 2017.

[22] J. O. Ighalo and O. A. Eletta, "Response surface modelling of the biosorption of Zn (II) and Pb (II) onto Micropogonias undulatus scales: Box–Behnken experimental approach," *Applied Water Science*, vol. 10, no. 8, pp. 1–12, 2020.

[23] J. Behin and N. Farhadian, "Response surface methodology and artificial neural network modeling of reactive red 33 decolorization by O3/UV in a bubble column reactor," *Advances In Environmental Technology*, vol. 2, no. 1, pp. 33–44, 2016.

[24] T. C. Egbosiuba, A. S. Abdulkareem, A. S. Kovo et al., "Adsorption of Cr(VI), Ni(II), Fe(II) and Cd(II) ions by KIAgNPs decorated MWCNTs in a batch and fixed bed process," *Scientific Reports*, vol. 11, no. 1, pp. 1–20, 2021.

[25] A. G. Adeniyi, J. O. Ighalo, and T. E. Odetoye, "Response surface modelling and optimisation of biodiesel production from avocado plant (Persea americana) oil," *Indian Chemical Engineer*, vol. 62, no. 3, pp. 243–250, 2020.

[26] A. Veved, G. W. Ejuh, and N. Djongyang, "Study of the chemical softness, chemical hardness, chemical stability and interaction energy of the piezoelectric composite," *Polymer Bulletin*, vol. 78, no. 9, pp. 4977–4986, 2021.

[27] Y. Cao, R. E. Malekshah, Z. Heidari, R. Pelalak, A. Marjani, and S. Shirazian, "Molecular dynamic simulations and quantum chemical calculations of adsorption process using amino-functionalized silica," *Journal of Molecular Liquids*, vol. 330, article 115544, 2021.

[28] E. V. Gómez, N. A. Ramírez Guarnizo, J. D. Perea, A. S. López, and J. J. Prías-Barragán, "Exploring molecular and electronic property predictions of reduced graphene oxide nanoflakes via density functional theory," *ACS Omega*, vol. 7, no. 5, pp. 3872–3880, 2022.

[29] N. Q. Su and X. Xu, "Insights into direct methods for predictions of ionization potential and electron affinity in density functional theory," *The Journal of Physical Chemistry Letters*, vol. 10, no. 11, pp. 2692–2699, 2019.

[30] V. Kalaipoonguzhali, K. Senthil Kannan, C. Thirumoorthi, M. Chinnadurai, and T. Jayanalina, "Comparison of adsorption energy, ionization potential and electron affinity of CuS-ACT and CuS-Nit nanostructures monowire for nano device fabrication by computational approach," *Materials Today: Proceedings*, vol. 33, pp. 2759-2760, 2020.

[31] K. A. Alshibli and M. B. Cil, "Influence of particle morphology on the friction and dilatancy of sand," *Journal of Geotechnical and Geoenvironmental Engineering*, vol. 144, no. 3, p. 04017118, 2018.

[32] X. Yang, Y. Wan, Y. Zheng et al., "Surface functional groups of carbon-based adsorbents and their roles in the removal of heavy metals from aqueous solutions: a critical review," *Chemical Engineering Journal*, vol. 366, pp. 608–621, 2019.

[33] Y. Cheng, R. Tan, W. Wang, Y. Guo, P. Cui, and W. Song, "Controllable synthesis and magnetic properties of Fe3O4 and Fe3O4@ SiO2 microspheres," *Journal of Materials Science*, vol. 45, no. 19, pp. 5347–5352, 2010.

[34] G.-H. Du, Z. Liu, X. Xia, Q. Chu, and S. Zhang, "Characterization and application of Fe3O4/SiO2 nanocomposites," *Journal of Sol-Gel Science and Technology*, vol. 39, no. 3, pp. 285–291, 2006.

[35] J. Ighalo, A. Adelodun, A. Adeniyi, and C. Igwegbe, "Modelling the effect of sorbate-sorbent interphase on the adsorption of pesticides and herbicides by historical data design," *Energy & Environment*, vol. 11, no. 4, pp. 253–259, 2020.

[36] A. Ghanim, "Optimization of pollutants removal from textile wastewater by electrocoagulation through RSM," *Journal of University of Babylon*, vol. 22, no. 2, pp. 375–387, 2014.

[37] Y. Rashtbari, F. Sher, S. Afshin et al., "Green synthesis of zerovalent iron nanoparticles and loading effect on activated carbon for furfural adsorption," *Chemosphere*, vol. 287, Part 1, article 132114, 2022.

[38] J. L. Martinez, "Environmental pollution by antibiotics and by antibiotic resistance determinants," *Environmental Pollution*, vol. 157, no. 11, pp. 2893–2902, 2009.

[39] C. Liu, V. Nanaboina, G. V. Korshin, and W. Jiang, "Spectroscopic study of degradation products of ciprofloxacin, norfloxacin and lomefloxacin formed in ozonated wastewater," *Water Research*, vol. 46, no. 16, pp. 5235–5246, 2012.

[40] M. J. Amiri, M. Bahrami, and F. Dehkhodaie, "Optimization of Hg (II) adsorption on bio-apatite based materials using CCD-RSM design: characterization and mechanism studies," *Journal of Water and Health*, vol. 17, no. 4, pp. 556–567, 2019.

[41] J. P. Maran, V. Sivakumar, K. Thirugnanasambandham, and R. Sridhar, "Artificial neural network and response surface methodology modeling in mass transfer parameters predictions during osmotic dehydration of Carica papaya L," *Alexandria Engineering Journal*, vol. 52, no. 3, pp. 507–516, 2013.

[42] J. Roslan, M. S. Kamal, M. K. Yunos, and N. Abdullah, "Optimization of enzymatic hydrolysis of tilapia (Oreochromis niloticus) byproduct using response surface methodology," *International Food Research Journal*, vol. 22, no. 3, p. 1117, 2015.

[43] A. Mohseni-Bandpi, T. J. Al-Musawi, E. Ghahramani, M. Zarrabi, S. Mohebi, and S. A. Vahed, "Improvement of zeolite adsorption capacity for cephalexin by coating with magnetic Fe_3O_4 nanoparticles," *Journal of Molecular Liquids*, vol. 218, pp. 615–624, 2016.

[44] Y. Rashtbari, S. Hazrati, S. Afshin, M. Fazlzadeh, and M. Vosoughi, "Data on cephalexin removal using powdered activated carbon (PPAC) derived from pomegranate peel," *Data in Brief*, vol. 20, pp. 1434–1439, 2018.

[45] R. J. Erb, "Introduction to backpropagation neural network computation," *Pharmaceutical Research*, vol. 10, no. 2, pp. 165–170, 1993.

[46] S. Sharma, S. Sharma, and A. Athaiya, "Activation functions in neural networks," *Towards Data Science*, vol. 6, no. 12, pp. 310–316, 2017.

[47] S. Chopra, D. Yadav, and A. Chopra, "Artificial neural networks based Indian stock market price prediction: before and after demonetization," *Journal of Swarm Intelligence and Evolutionary Computation*, vol. 8, no. 174, 2019.

[48] S. Chen and H. Wang, "SAR Target Recognition Based on Deep Learning," in *2014 International Conference on Data Science and Advanced Analytics (DSAA)*, Shanghai, China, 2014IEEE.

[49] F. Aslam, F. Farooq, M. N. Amin et al., "Applications of gene expression programming for estimating compressive strength of high-strength concrete," *Advances in Civil Engineering*, vol. 2020, Article ID 8850535, 23 pages, 2020.

[50] A. Hasni, A. Sehli, B. Draoui, A. Bassou, and B. Amieur, "Estimating global solar radiation using artificial neural network and climate data in the south-western region of Algeria," *Energy Procedia*, vol. 18, pp. 531–537, 2012.

[51] H. Esen, M. Inalli, A. Sengur, and M. Esen, "Forecasting of a ground-coupled heat pump performance using neural networks with statistical data weighting pre-processing," *International Journal of Thermal Sciences*, vol. 47, no. 4, pp. 431–441, 2008.